Flow Transition within an Evaporating Binary Mixture Sessile Drop

John R. E. Christy,[1,*] Yoshinori Hamamoto,[1,2] and Khellil Sefiane[1]

[1]School of Engineering, The University of Edinburgh, Kings Buildings, Edinburgh EH9 3JL, United Kingdom
[2]Department of Mechanical Engineering, Kyushu University, Fukuoka 819-0395, Japan

(Received 22 December 2010; revised manuscript received 31 March 2011; published 17 May 2011)

The flow field along the base of an evaporating ethanol-water droplet and its evolution time was measured by particle image velocimetry. Three stages are revealed, a first stage dominated by multiple vortices, a second transition stage characterized by a remarkable spike in outward flow not previously identified, and a third stage dominated by outward flow identical to that found for pure water. Stage I is thought to be driven by surface tension gradients arising from local concentration variation. The spike in outward flow is explained in terms of a transition corresponding to almost total depletion of ethanol. An exponential decay in vorticity during the transition stage is explained in terms of ethanol diffusion from the bulk to the interface. We speculate on the existence of a zero-concentration wave propagating from the apex to the contact line corresponding to the final total depletion of ethanol.

DOI: 10.1103/PhysRevLett.106.205701 PACS numbers: 64.60.Ej, 47.20.Dr, 64.70.F−, 68.03.Cd

Introduction.—The evaporation and wetting of pure droplets has been extensively studied in recent years [1–4]. This interest is driven by many technological and biological applications for this seemingly simple phenomenon; e.g., the evaporation of blood serum drops has recently been introduced as a diagnostic tool for certain diseases [5]. The use of drying droplets for nanopatterning deposition [6] and DNA stretching [7] are a few examples of recent developments in this area. However, much less work has been done on the evaporation of multicomponent droplets.

For pure droplets, the behavior of the drop depends on the wettability and roughness of the surface. When first formed, the contact angle of the liquid will usually be close to the advancing contact angle. The drop will often remain pinned until the receding contact angle is reached, after which, on smooth surfaces, the contact line will tend to slide with constant contact angle. On rough surfaces the drop usually remains pinned and the contact angle will continue to decrease. Sometimes both the contact angle and drop diameter will decrease simultaneously or the drop will go through a sequence of depinning and pinning such that the drop radius jumps through a number of discrete values. For water drops [8], we have measured the horizontal component of the velocity within the drop and shown it to be consistent with mass conservation to account for preferential evaporation at the contact line as predicted by Deegan *et al.* [9].

With droplets formed from binary mixtures of an alcohol (methanol [10], ethanol [11–14], and 1-propanol [15]) and water, the behavior is generally different, particularly for mixtures on the water-rich side of any binary azeotrope [15]. Depending on the wettability and smoothness of the surface there may be an initial phase during which the drop remains pinned and the contact angle decreases. This is followed on smooth surfaces by a phase in which the contact angle increases, from a value more representative of the alcohol to a value close to that found with pure water drops. Rowan *et al.* [15] found it difficult to take measurements during this phase for propanol-water mixtures on polymethylmethacrylate. During this phase the contact line slides to allow this angle to increase. There may then follow a period where the contact angle remains constant with the contact line sliding or the contact angle will then start to decrease with or without change in the drop radius. For pinned binary drops (as reported in this Letter), the contact angle decreases throughout, but the change in characteristics at the contact line is observed in terms of a change in the evaporation rate (Fig. 1).

It is thought that most of the alcohol evaporates during the first two stages described above, leaving behind a liquid that is almost pure water, so that the final stages of evaporation mirror those of a pure water sessile droplet.

So far, all investigators are agreed that the evaporation can be divided into a period during which the alcohol preferentially evaporates, followed by evaporation of almost pure water. However, as yet no one has studied the interior flow in such drops to gain an understanding of how the fluid mechanics impinge on the evaporation process. We have therefore addressed this issue in an attempt to

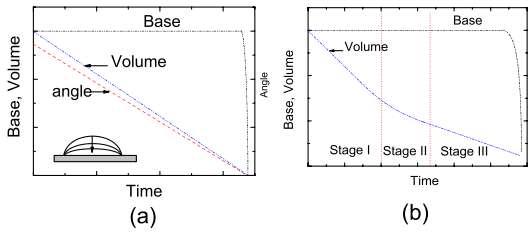

FIG. 1 (color online). Evolution of profile during the evaporation of (a) a pure sessile drop and (b) a binary drop for pinned drops.

elucidate the mechanisms governing the various stages outlined above.

Experimental results and discussion.—Particle image velocimetry was used to obtain velocity information within evaporating sessile drops. 0.12 μl ($\pm$ 0.03 μl) droplets of 5% vol ethanol, 95% vol distilled water, seeded with 0.04% solids of fluorescent microspheres (1 μm diameter, Nile-red, carboxylate modified FluoSphere® beads of density 1.05 g/cm^3) were injected onto a clean glass cover slide, sitting on an inverted microscope (Leica DM15000 M) to yield sessile drops of about 1.25 mm diameter. Because of the presence of particles in the fluid, the contact line remained pinned throughout. A New Wave Pegasus pulse diode laser emitting at 527 nm, synchronized with a Dantec Dynamics Nanosense II camera (512 $\times$ 512 pixels) at 20 Hz, was used to cause the particles to fluoresce at 575 nm and the resulting images captured. The resolution of the images was 320 pixels/mm. The height, above the base of the drop, of the plane in which the velocities were determined was set by adjusting the focus on the microscope. For all results reported here, the height was approximately 10 μm off the base of the drop, and the depth of field of the microscope lens was approximately 20 μm. Velocities of the particles in the horizontal plane were determined by cross correlation of successive images [16,17], for 16 $\times$ 16 interrogation windows with 50% overlap to yield a 63 $\times$ 63 vector array, using Dantec Dynamics Flowmanager 4.71 software. A peak validation algorithm was performed with vectors rejected if the tallest correlation peak was less than 1.2 times the second peak. Typically, up to one-quarter of the vectors were rejected at this stage.

Velocity maps were created from image pairs for every 0.5 s over the lifetime of the drop and for every 0.05 s over the region where the flow pattern was changing. From the velocity map, vorticity around a vertical axis could be evaluated. Prior to calculating the vorticity a moving average filter was applied, substituting vectors by an average based on an 11 $\times$ 11 array centered on the vector position, before a mask was used to exclude any spurious vectors outside the edge of the drop. The vorticity around an axis perpendicular to the image plane at position m, n was calculated from $\omega_z = \frac{v_{(m+1,n)y} - v_{(m-1,n)y}}{2\Delta x} - \frac{v_{(m,n+1)x} - v_{(m,n-1)x}}{2\Delta y}$, where Δx and Δy are the grid spacing. The vorticity is shown in terms of color coding on the velocity vector maps in Fig. 2.

Three distinct phases of flow behavior were observed, as depicted in Figs. 2–4. In the first stage (I), a number of vortices are present in the fluid, which appear to have random orientation and number (up to eight distinct vortices were observed), though the spatial average vorticity remains roughly constant at about 0.35 s^{-1}. There is some evidence of oscillation of these vortices, revealed also in fluctuation of the average intensity. In the third stage (III), the flow is radially outwards, with virtually zero vorticity around the vertical axis, and the velocity increases rapidly

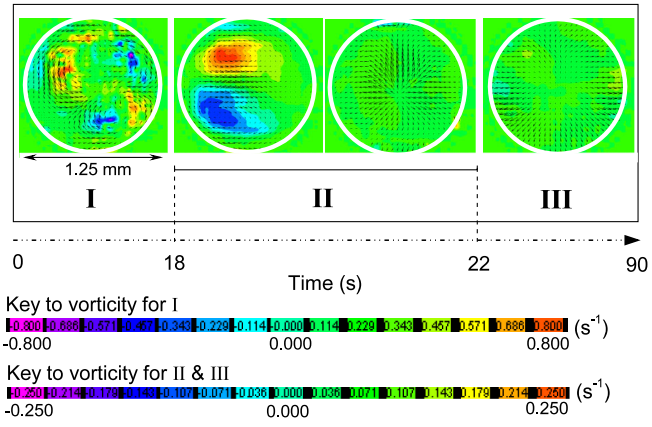

FIG. 2 (color online). Particle image velocimetry results showing flow field in terms of velocity vectors and vorticity for the three identified evaporation stages.

towards the end of the lifetime of the drop, as was found for evaporation of pure water drops [8]. This flow can be explained in terms of mass conservation due to preferential evaporation at the contact line. Between stages I and III, we have a transition stage (II), in which the vorticity decays exponentially towards zero with time [Fig. 4 inset (a)]. During this stage, the fraction of the drop area having vorticity (a threshold of 0.05 s^{-1} is adopted) also drops rapidly as can be seen in Fig. 4 inset (b), which shows a correlation between the intensity of the vortices and the fraction of the area they occupy. This is accompanied by migration of the remaining vortices towards the outer edge of the drop. During this transition stage, we also observed a remarkable spike in the radial velocity (Fig. 3) as the vorticity was undergoing its exponential decay. Exactly the same flow behavior has been observed also for droplets

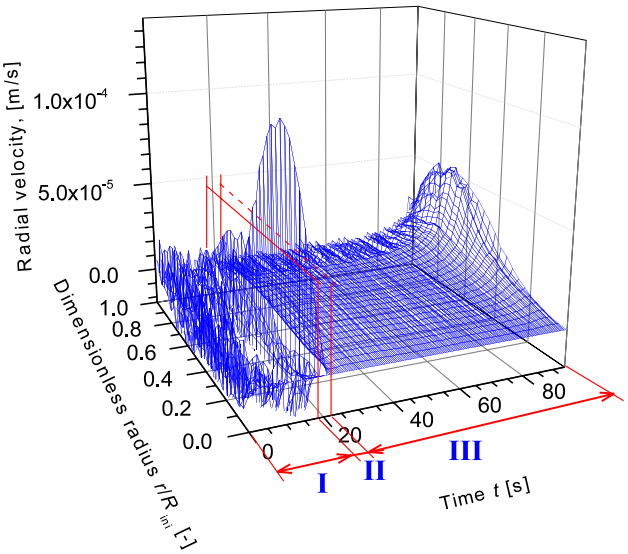

FIG. 3 (color online). 3D map showing the evolution of averaged velocity in time along the radial position. The three phases are clearly identified.

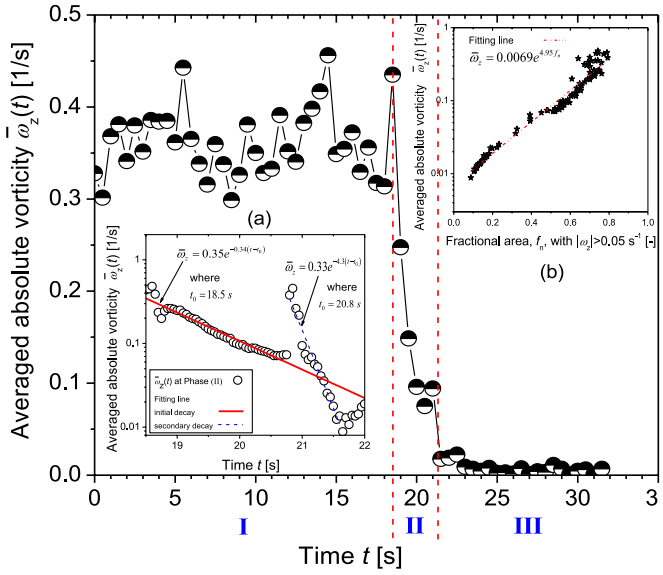

FIG. 4 (color online). Spatially averaged vorticity versus time. Insets show semilog plots of (a) the averaged vorticity in time and (b) the averaged vorticity as a function of the fractional area whose vorticity exceeds a threshold of 0.05 s^{-1}, both for the transition stage (stage II).

with initial ethanol concentrations of 25% vol and 50% vol and with two acquisition frequencies (20 and 100 Hz). Consistently we observe the same stages and transition characteristics as described above.

The presence of multiple vortices in the first phase suggests that the internal flow at this stage is driven either by concentration or temperature gradients and not simply by evaporative flux, since evaporation is known to be greatest in the region of the contact line, which would lead to a radially outward flow. Cheng *et al.* [12], although unable to take measurements during this phase because of the instabilities in contact line behavior, postulate that the instabilities are driven by temperature gradients, citing the work of Hopkins and Reid [18] on temperature variations in evaporating aerosol drops of alcohol-water mixtures. We have used infrared thermography on our sessile drops and observed very little temperature difference at the surface of the drop, so we believe that these vortices may be driven by concentration gradients, most likely through the effect of concentration on the local surface tension, though it is possible that even small variations in temperature, perhaps themselves the result of differential evaporation due to concentration variation, may also lead to surface tension gradients. Dehaeck *et al.* [19] have demonstrated how concentration gradients in evaporation of ethanol-water mixtures can lead to buoyancy-driven convection in a Hele-Shaw cell. It should be noted, however, that the length scales over which initial gradients were measured in their experiment were larger than the size of our drops. For our experiments, surface tension effects arising from concentration gradients are likely to dominate buoyancy effects.

In summary, in order to elucidate the nature and driving mechanisms of the observed flow we considered all of the possible physical mechanisms: (a) gravity driven due to density difference, (b) mass conservation due to evaporative loss, and (c) surface tension driven due to temperature or concentration variation at the surface. Since our drops are smaller than the capillary length we disregarded gravity driven flows. Mass conservation flows are characterized by radially outward flows as reported by Deegan [9] and demonstrated by our recent experiments [8]. The surface tension driven flows can be the result of either temperature or concentration variation. By elimination, we concluded that the multiple vortices are most probably driven by composition variations.

The radial flow in stage III shows exactly the same characteristics as that measured by us for pure water [8]. The flow is radially outwards and there is both a rise in radial velocity spatially towards the contact line and a dramatic rise in the radial velocity temporally towards the end of the drop lifetime. The magnitude of the velocities is also similar, being consistent with mass conservation to match the evaporative flux near the contact line. Our experiments therefore confirm the observations made previously that the majority of the alcohol evaporates in the early stages of the evaporation process.

Stage II is of most interest, revealing for the first time details of the transition between the highly disturbed ethanol evaporation regime and that of the evaporation of residual water. Here there are two hitherto unseen characteristics, which shed some light on the mechanisms of transfer within the drop. The first is an exponential decay in the vorticity with time, accompanied by a migration of the remaining vorticity towards the outer edge of the drop and the second is a truly remarkable spike in the radial flow, much too large to be explained by evaporative flux alone, just before the flow settles down to that of a pure water drop.

The exponential decay in the second phase may be explained as follows: During the first phase the intense vorticity leads to uniformity of ethanol concentration throughout the drop, with convective transfer of ethanol to the drop surface, where it preferentially evaporates. We believe that the vortices are fed by local surface tension gradients induced by gradients in the ethanol concentration at the surface. As we noted earlier, infrared thermography did not reveal significant temperature variations that might also lead to surface tension gradients. The surface tension gradients, which would be proportional to the concentration gradients, result in an applied stress, which for a laminar flow result in a velocity, $\underline{u}$, proportional to the stress. The average vorticity, curl($\underline{u}$), will be proportional to this velocity and hence to the concentration gradient. In other words, we expect $\bar{\omega}_z \propto \nabla C_{\text{ethanol}}$. Once the concentration of ethanol drops in the bulk, the concentration of ethanol at the surface also drops and the driving force for the vortices starts to decrease. This reduction in concentration leads to molecular diffusion becoming the more dominant mechanism for the transfer of ethanol to the

surface, and particularly the area of the surface close to the contact line where evaporation is greatest. For diffusion, $\frac{\partial C_{\text{ethanol}}}{\partial t} = D\frac{\partial^2 C_{\text{ethanol}}}{\partial x^2}$. If we also assume that $C_{\text{ethanol}} \cong 0$ at the contact line, then by separation of variables [20], a solution of the form $C_{\text{ethanol}} = \frac{4C_0}{\pi} \times \sum_{n=0}^{\infty} \frac{1}{2n+1} \sin(\frac{(2n+1)\pi x}{d}) \exp\{\frac{-D(2n+1)^2\pi^2 t}{d^2}\}$ is obtained (where d is the drop diameter and C_0 is the concentration at zero time) which would result in the average concentration decaying exponentially with time. Assuming the concentration gradient, $\nabla C_{\text{ethanol}}$ close to the contact line to be proportional to $\frac{C_{\text{ethanol}}-0}{d}$, this gives $\nabla C_{\text{ethanol}} = \nabla C_{\text{ethanol},0} e^{-kt}$, where t is measured from the start of the decay. If $\bar{\omega}_z \propto \nabla C_{\text{ethanol}}$, this would lead to $\bar{\omega}_z = \bar{\omega}_{z,0} e^{-kt}$, which is in agreement with the trend shown in Fig. 4.

The sudden spike in radial velocity, observed in our velocity map as a symmetrical radial flow towards the contact line, may be associated with the formation of a single toroidal vortex. The velocity is more than an order of magnitude higher than that associated with the velocity expected due to fluid evaporation at the contact line, so mass conservation would require an associated inward flow in the upper region of the drop, such as would occur if the surface tension near the apex became significantly greater than that near the contact line. Such a situation could arise if the apex of the drop became almost totally depleted of ethanol, while the surface in the outer region of the drop continues to have ethanol present. Since our observation is that vortices die out first near the apex, this may explain how such a situation could arise. Without vortices close to the apex, replenishment of ethanol at the surface following local evaporation would be by molecular diffusion, whereas vortices will continue to ensure that ethanol is convected to the surface near the contact line. This difference in efficiency of transfer of ethanol to the surface could lead to a significant concentration gradient and the resultant peeling back of the surface. Following the proposed scenario, we speculate on the existence of a zero-concentration wave which starts at the apex of the drop and propagates toward the edge. Indeed the total depletion of ethanol must start somewhere in the drop; it is likely that the last ethanol molecules will be concentrated near the interface, the zero-concentration wave propagation would correspond to the total depletion of ethanol which seems to start at the apex of the drop.

From the inset in Fig. 4 it is clear that there are two distinct exponential decay curves. The first has a slope of 0.78 s^{-1} and the second a slope of 4.3 s^{-1}. From these slopes we can calculate diffusion times of 1.3 and 0.23 s, respectively, which with a diffusion constant for ethanol in water of 1.5×10^{-9} m^2/s leads to diffusion lengths $(= \sqrt{D\tau})$ of 4×10^{-5} and 2×10^{-5} m, respectively. There is a clear discontinuity between these curves. This discontinuity occurs at the same time as the spike in velocity. We speculate that the second, more rapid decay in vorticity is driven by viscosity in the absence of ethanol diffusion to the surface to sustain concentration gradients, occurring once the ethanol runs out These figures for the diffusion length are consistent in magnitude with those observed by Dehaeck *et al.* [19] during their experiments.

In conclusion, we show that the flow within evaporating binary mixture droplets goes through three distinct stages. The first is a chaotic regime characterized by vortices possibly driven by concentration differences arising during the preferential evaporation of ethanol. The second, transition regime, sees an exponential decay in the vorticity with the remaining vortices migrating towards the contact line, accompanied by a spike in the radial velocity along the base of the drop, perhaps due to depletion of ethanol in the drop surface close to the apex of the drop leading to a surface tension instability. The third stage is characterized by radial flow towards the contact line to match the evaporative flux and is identical to the flow measured by us for pure water drops.

*Corresponding author.
J.Christy@ed.ac.uk

[1] K. Sefiane *et al.*, Phys. Fluids **21**, 062101 (2009).
[2] G. Dunn *et al.*, J. Fluid Mech. **623**, 329 (2009).
[3] H. Hu and R. G. Larson, Langmuir **21**, 3972 (2005).
[4] H. Ghasemi and C. A. Ward, Phys. Rev. Lett. **105**, 136102 (2010).
[5] T. A. Yakhno *et al.*, Tech. Phys. **48**, 399 (2003).
[6] R. Craster, O. K. Matar, and K. Sefiane, Langmuir **25**, 3601 (2009).
[7] V. Dugas, J. Broutin, and E. Souteyrand, Langmuir **21**, 9130 (2005).
[8] Y. Hamamoto, J. R. E. Christy, and K. Sefiane, Phys. Rev. E **83**, 051602 (2011).
[9] R. D. Deegan *et al.*, Nature (London) **389**, 827 (1997).
[10] K. Sefiane, S. David, and M. E. R. Shanahan, J. Phys. Chem. B **112**, 11 317 (2008).
[11] K. Sefiane, L. Tadrist, and M. Douglas, Int. J. Heat Mass Transf. **46**, 4527 (2003).
[12] A. K. H. Cheng, D. M. Soolaman, and H. Yu, J. Phys. Chem. B **110**, 11 267 (2006).
[13] C. Liu and E. Bonaccurso, Rev. Sci. Instrum. **81**, 013702 (2010).
[14] L. X. Shi *et al.*, Surf. Interface Anal. **41**, 951 (2009).
[15] S. M. Rowan *et al.*, J. Phys. Chem. B **104**, 8217 (2000).
[16] R. D. Keane and R. J. Adrian, Appl. Sci. Res. **49**, 191 (1992).
[17] C. E. Willert and M. Gharib, Exp. Fluids **10**, 181 (1991).
[18] R. J. Hopkins and J. P. Reid, J. Phys. Chem. B **110**, 3239 (2006).
[19] S. Dehaeck, C. Wylock, and P. Colinet, Phys. Fluids **21**, 091108 (2009).
[20] J. Crank, *The Mathematics of Diffusion* (Oxford University Press, Oxford, 1975), 2nd ed.